Applied Thermal Engineering 56 (2013) 152–158

Contents lists available at SciVerse ScienceDirect

Applied Thermal Engineering

journal homepage: www.elsevier.com/locate/apthermeng

Modeling passive power generation in a temporally-varying temperature environment via thermoelectrics

Cory C. Bomberger [a], Peter M. Attia [b], Ajay K. Prasad [c], Joshua M.O. Zide [a,c,*]

[a] Department of Materials Science and Engineering, University of Delaware, Newark, DE 19716, USA
[b] Department of Chemical and Biomolecular Engineering, University of Delaware, Newark, DE 19716, USA
[c] Department of Mechanical Engineering, University of Delaware, Newark, DE 19716, USA

HIGHLIGHTS

- Thermoelectric power generation with time-varying temperature is modeled.
- The ability to generate power without a natural spatial gradient is demonstrated.
- Time dependent heat-transfer and differential heat flow rates are considered.
- Optimization of power generation via scaling the device size is discussed.

ARTICLE INFO

Article history:
Received 19 November 2012
Accepted 27 February 2013
Available online 14 March 2013

Keywords:
Thermoelectrics
Heat exchangers
Time-varying temperature gradient
Power optimization
Convective heat transfer
Radiative heat transfer

ABSTRACT

This paper presents a model to predict the power generation of a thermoelectric generator in a temporally-varying temperature environment. The model employs a thermoelectric plate sandwiched between two different heat exchangers to convert a temporal temperature gradient in the environment to a spatial temperature gradient within the device suitable for thermoelectric power generation. The two heat exchangers are designed such that their temperatures respond to a change in the environment's temperature at different rates which sets up a temperature differential across the thermoelectric and results in power generation. In this model, radiative and convective heat transfer between the device and its surroundings, and heat flow between the two heat exchangers across the thermoelectric plate are considered. The model is simulated for power generation in Death Valley, CA during the summer using the diurnal variation of air temperature and radiative exchange with the sun and night sky as heat sources and sinks. The optimization of power generation via scaling the device size is discussed. Additional applications of this device are considered.

1. Introduction

Thermoelectric generators are promising for the direct conversion of thermal energy to electrical energy. The efficiency of this conversion is proportional to a dimensionless figure of merit ZT given by $ZT = \sigma\alpha^2 T/\kappa$, where σ is the electrical conductivity, α is the Seebeck coefficient, T is the operating temperature, and κ is the thermal conductivity. The figure of merit increases with increasing electrical conductivity and decreasing thermal conductivity; however, the thermal conductivity has a lattice contribution and an electronic contribution, which is related to the electrical conductivity by the Wiedemann–Franz law [1]. Thus, ZT is usually below 1, and thermoelectric generators have a low efficiency and are thus generally considered for applications where efficiency is not a priority [2]. Efficiency is not a priority when the cost of operation is small or nonexistent, such as when the source of heat is naturally occurring, as in solar heat [3–6] and gradients in ocean temperatures [7]. Another case when efficiency is not a priority is when the thermal gradient used by the thermoelectric generator is produced as waste heat from another process [8]. There has been extensive analysis of waste-heat recovery using thermoelectric power generators [9] with specific studies on using waste heat in a steam-based power plant [10] and waste heat in automobiles [11].

Most of the studies mentioned above are done by modeling a thermoelectric in a specific application. When analyzing the power output of a thermoelectric module, the material and geometry choice of each part of the device will affect the power output as well as the thermal losses considered. A thermoelectric power generator

* Corresponding author. Department of Materials Science and Engineering, University of Delaware, 201 Dupont Hall, Newark, DE 19716, USA. Tel.: +1 302 831 3244; fax: +1 302 831 4545.
E-mail address: zide@udel.edu (J.M.O. Zide).

1359-4311/$ – see front matter © 2013 Elsevier Ltd. All rights reserved.
http://dx.doi.org/10.1016/j.applthermaleng.2013.02.039

device consists of three major parts: two heat exchangers sandwiching a thermoelectric module. Several studies have investigated the impact of the heat exchanger geometry on power output in a variety of applications [7,12–14]. A thermoelectric module in its simplest form is composed of a *p*-type doped semiconductor and a *n*-type doped semiconductor connected electrically in series, mechanically supported by thin ceramic plates. For low temperature operation, bismuth telluride semiconductors are the dominant semiconductors because of their relatively high efficiency. In recent years, advances have been made in other material systems such as systems based on iron alloys where the materials are more abundant, silicon thermoelectrics, and semiconductors with buried semi-metallic nanoparticles [10,15–17]. Additionally, the geometry of the thermoelectric module, such as thin films, cylindrical modules, multiple elements, and multi-stage modules, can affect the power output [18–22]. When modeling the effect of heat exchangers and thermoelectric geometries on power output, the choice of heat transfer mechanisms considered, both internal and external, is important [23,24].

While thermoelectrics are typically used for power generation when the operating costs are low or negligible, optimization studies and cost analysis are valuable to maximize power output and determine the economic feasibility of thermoelectric power generation. Many studies have optimized the power and efficiency of thermoelectric devices [21,25,26] with specific studies for small temperature gradients [27,28] and waste heat applications [29,30]. While the cost of running a thermoelectric power generator is small or negligible in most cases, the cost of materials and manufacturing these devices can limit the commercial feasibility. Several analyzes have determined the cost of thermoelectric energy production when material and manufacturing costs have been minimized [8,29–31]. The practicality of thermoelectric power generation is determined by combining these cost and optimization studies.

In this paper, we present a model of a thermoelectric plate sandwiched between two different heat exchangers placed in an environment where the temperature varies temporally with the goal to harvest energy from systems where spatial gradients are not otherwise available. The diurnal ambient temperature variation represents one example of this type of environment. In this system, the heat exchangers are designed such that their temperatures respond to a change in the environment's temperature at different rates. The difference in the thermal response rates between the two heat exchangers sets up a temperature differential across the thermoelectric, which then can be exploited for power generation. In such a system, it would be possible for the hot and the cold sides of the thermoelectric to switch during the temperature cycle, resulting in a reversal of the direction of heat flow across the thermoelectric. In this case, the device would continue to generate electric power, except that the direction of the DC current flow from the thermoelectric would undergo a concurrent reversal [2].

2. Model description

2.1. System specification

In this numerical analysis, a thermoelectric plate is sandwiched between two different heat exchangers, shown in Fig. 1. The heat exchangers are designed such that one has a large thermal mass (HE1) and the other a small thermal mass (HE2), allowing the temperature of HE1 to remain relatively constant while the temperature of HE2 responds quickly to fluctuations in the environment's temperature. With these design constraints considered, HE1 is chosen to be a truncated quartz sphere, allowing a flat top for good thermal contact with the thermoelectric device. The thermoelectric device consists of 254 elements in a 16 by 16 array, with two elements removed to allow for electrical contacts. Each element has a length of 3.11 mm corresponding to the thickness of the thermoelectric (see the inset in Fig. 1). The thickness of the thermoelectric was determined based on a fill factor of 1 and the optimization of the power output [27,31].

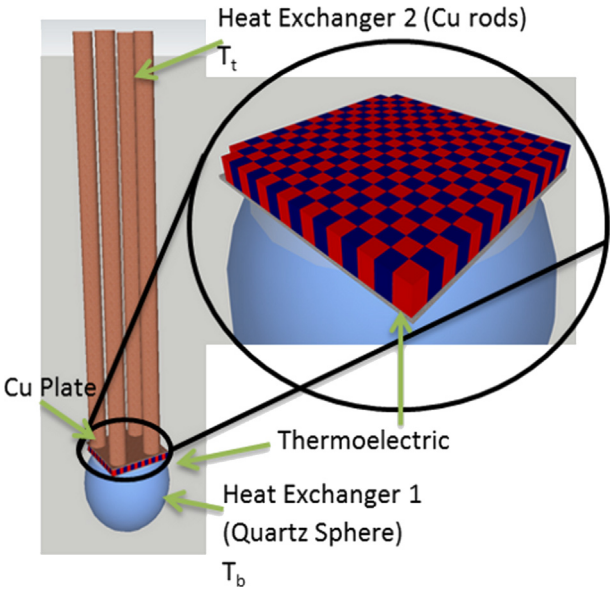

Fig. 1. A schematic of the device setup. Heat exchanger 1 is the sphere below the thermoelectric plate, with a temperature of T_b. Heat exchanger 2 is the rod array and copper plate assembly mounted to the top of the thermoelectric plate, with a temperature of T_t. The inset shows the array of thermoelectric elements that make up the thermoelectric module.

Thermoelectric elements are generally sandwiched between two ceramic plates for mechanical stability; in this model, we neglect the ceramic plates. The ceramic plates lie at the interface between the heat exchangers and the thermoelectric module. Thus, at any given instant in time, they would reduce the temperature differential across the thermoelectric and reduce the output power at that time. However, by introducing additional thermal resistance, the ceramic plates would help to insulate the two heat exchangers from each other and maintain their temperature differential, extending the time period over which power is produced. Thus, neglecting the ceramic plates lead to a slight overestimation of the power output at any given time, but the time period over which power is produced is somewhat conservative. Since the ceramic plates have much higher thermal conductivity compared to the thermoelectric elements, we believe these effects to be relatively small.

The other side of the thermoelectric device is thermally bonded to HE2. HE2 consists of an array of copper rods configured to maximize heat transfer with the surroundings mounted on a copper plate that spreads the heat from the copper rods laterally over the surface of the thermoelectric, and vice versa. In this setup, HE1 is on the bottom and HE2 is on the top. The material properties for HE1 and HE2 are shown in Table 1 [32–35]. The performance of the thermoelectric power generation is limited by one of the semiconductors, the *n*- or *p*-type [20]. This model uses the materials properties of the *p*-type Bi_2Te_3 because it performs slightly worse than *n*-type Bi_2Te_3, resulting in a conservative power output estimate. *P*-type Bi_2Te_3 has a thermal conductivity of 2.06 W m^{-1} K^{-1}, Seebeck coefficient of 162 μV K^{-1}, and electrical resistivity of 5.5 μΩ m [18,36].

Table 1
Material properties of HE1 and HE2 [32–35].

	Material	Thermal conductivity κ (W m^{-1} K^{-1})	Specific heat C_p (J mol^{-1} K^{-1})	Density ρ (g cm^{-3})	Absorptivity a	Emissivity e
HE1	Quartz	1.4	44.2	2.635	–	–
HE2	Copper	401	24.6	8.96	0.7	0.78

In this simulation, the device is assumed to be operating during the summer in an environment similar to that of Death Valley, CA. Based on this location, the temperature of the air fluctuates sinusoidally with a maximum of 321 K occurring at 2 p.m. and a minimum of 293 K occurring at 2 a.m. The fluid surrounding the device is assumed to be dry air with constant properties given in Table 2 [37]. It is assumed that the air is moving at a constant velocity of 0.894 m s^{-1}, there is no temperature gradient within the fluid, and any heat transferred from the device to the fluid has a negligible effect on the fluid's temperature. Due to the small temperature range, it is assumed that the properties of HE1, HE2, the thermoelectric device, and the air do not change with time.

2.2. Numerical model

This model considers three modes of heat transfer: convection between the air and HE1 and HE2, heat flow between HE1 and HE2 (across the thermoelectric), and radiation between HE2 and the sun or night sky. Conduction between the device and the earth is neglected by assuming a thermally isolating stand to hold the device above the earth; this stand would make minimal contact with the device resulting in a negligible amount of heat transfer between the stand and the device. Additionally, due to the small contact area, the stand would not inhibit the device's ability to exchange heat with the air. In some plausible applications, the contact between the device and the environment can be minimized as in the current implementation. In other situations, any physical contact between the device and surrounding material will affect the heat transfer process. Such an effect can be estimated only after the specific material and the exact nature of the contact are known. Our goal here is to present the simplest situation where such contact is minimized.

A lumped-parameter analysis is implemented such that thermal gradients within the solid bodies may be neglected. The Biot number is used to assess the validity of the lumped-parameter analysis. The Biot number is given as $\mathrm{Bi} = hR/\kappa$ where h is the heat transfer coefficient between the body and the surroundings, R is the characteristic length scale of the body, and κ is its thermal conductivity. For true lumped-parameter behavior, Bi must be much less than 1. The Biot number is reported for each simulation in Section 3.

The rate of heat flow is calculated assuming the temperature difference between two time steps (dT) is insignificant. The time step was selected to be less than τ, where

$$\tau = \frac{R^2 \rho C_p}{\kappa \mathrm{MW}} \tag{1}$$

Here, R is a characteristic length, ρ is the density, C_p is the molar heat capacity at constant pressure, κ is the thermal conductivity, and MW is the molecular weight.

Table 2
Material properties of the air [35].

Material	Thermal conductivity κ (W m^{-1} K^{-1})	Prandtl number Pr	Kinematic viscosity ν (m^2 s^{-1})	Velocity V (m s^{-1})
Dry air	0.03003	0.697	2.056×10^{-5}	0.894

The governing equations of the rate of convective heat transfer between the fluid and the bottom and top heat exchangers, respectively, are

$$\dot{Q}_{fb} = h_b A_{fb} (T_f - T_b) \tag{2}$$

$$\dot{Q}_{ft} = n h_t A_{ft} (T_f - T_t) \tag{3}$$

where A_{fb} and A_{ft} are the surface areas of HE1 and each rod in HE2 that is exposed to the fluid, respectively [38,39], and n is the number of rods in HE2. The heat transfer coefficients for the bottom and top heat exchangers are given by the following equations:

$$h_b = \frac{\mathrm{Nu}_b \kappa_f}{R_b} \tag{4}$$

$$h_t = \frac{\mathrm{Nu}_t \kappa_f}{R_t} \tag{5}$$

where κ_f is the thermal conductivity of the air, and R_b and R_t are the radii of the sphere and one rod, respectively. The Nusselt numbers are calculated as follows:

$$\mathrm{Nu}_b = 2 + 0.6 \mathrm{Re}_b^{0.5} \mathrm{Pr}^{1/3} \tag{6}$$

$$\mathrm{Nu}_t = \left(0.376 \mathrm{Re}_t^{0.5} + 0.057 \mathrm{Re}_t^{2/3}\right) \mathrm{Pr}^{1/3} + 0.92 \left(\log \frac{7.4055}{\mathrm{Re}_t} + 4.18 \mathrm{Re}_t\right)^{-1/3} \mathrm{Re}_t^{1/3} \mathrm{Pr}^{1/3} \tag{7}$$

where the Reynolds numbers are calculated using

$$\mathrm{Re}_b = \frac{V_f R_b}{\nu_f} \tag{8}$$

$$\mathrm{Re}_t = \frac{V_f R_t}{\nu_f} \tag{9}$$

where V_f is the air velocity, and ν_f is its kinematic viscosity [38,39].

Radiative heat transfer between the device and its surroundings was considered only for the case of radiative heat transfer from the sun and space to HE2. The rods in HE2 are arranged so they do not shade each other, allowing maximum radiative heat transfer with HE2. Due to the geometry of the device, it was assumed that HE2 shades the thermoelectric module and HE1 from exposure to the sun and the sky preventing radiative interactions. Additional shading can also be provided to eliminate radiative heat transfer between the sun or sky and the thermoelectric module or HE1. It was also assumed that the temperatures of the earth and any nearby objects were close enough to the temperature of the heat exchangers such that radiative heat transfer can be neglected. Sun angle data for Death Valley from a Nautical Almanac during the summer were fitted to a sinusoidal function to determine the radiation between the sun, sky, and HE2 as a function of time [34,39–41]. The radiative flux between the sun and HE2 during the day in kilowatts is given by

$$\dot{Q}_{st} = na_t A_{st}\left(C_0 + C_1 \sin\frac{\pi(t+C_2)}{C_3}\right) \quad (10)$$

where a_t and A_{st} are absorptivity and the area seen by the sun of each rod in HE2 respectively, t is time measured in seconds from 9:00 a.m. and C_0, C_1, C_2, and C_3 are fitting parameters given in Table 3 based on the angle of the sun as a function of time. A_{st} is given by

$$A_{st} = 2R_t H_t + \pi R_t^2 \quad (11)$$

where R_t and H_t are the radius and height, respectively, of each rod in HE2. The radiative flux between HE2 and the sky is given by

$$\dot{Q}_{nt} = nA_{nt}\sigma e_t\left(T_n^4 - T_t^4\right) \quad (12)$$

where A_{nt} is the area of each rod seen by the night sky, and e_t is the emissivity of HE2. A_{nt} is given by

$$A_{nt} = 2\pi R_t H_t + \pi R_t^2 \quad (13)$$

where R_t and H_t are the radius and height, respectively, of each rod in HE2. A_{st} and A_{nt} differ because at any instance the sun only sees one side and the top of the rod while all sides and the top of a rod are viewable by the night sky.

The foregoing discussion pertained to heat exchange between the two bodies and their surroundings. Next, we focus on heat transfer from HE1 to HE2. There are two modes of heat transfer between HE1 and HE2: heat flow by conduction across the thermoelectric plate and direct heat flow via radiation. Because the view factor between the two heat exchangers is approximately zero, radiation between HE1 and HE2 is neglected. The rate of heat flow between the heat exchangers and the thermoelectric module is given by summing the rate of heat flows due to conduction, Peltier heat transfer, Joule heating, and the Thomson effect. The rate of heat transfer across the thermoelectric by conduction is

$$\dot{Q}_{\text{cond}} = \frac{\left(\kappa_e A_e N + \kappa_f(A_m - NA_e)\right)(T_t - T_b)}{L_e} \quad (14)$$

where A_e, κ_e, and L_e are the area, thermal conductivity, and thickness of one thermoelectric element, respectively, and A_m is the area of the entire thermoelectric plate (which is equal to $(N+2)A_e$ for a fill factor of 1). The Peltier heat flux into and out of HE1 and HE2 are given by Eqs (15) and (16), respectively

$$\dot{Q}_{\text{PeltierHE1}} = N\alpha T_b I \quad (15)$$

$$\dot{Q}_{\text{PeltierHE2}} = -N\alpha T_t I \quad (16)$$

where α is the Seebeck coefficient, and T is the temperature of the heat exchanger in question at the time of interest. When the external resistance is load-matched to the internal resistance, the current is given by

Table 3
Fitting parameters for radiative exchange between HE2 and the sun, based on the angle of the sun as a function of time on July 10th, 11th, and 12th [40,41].

C_0	C_1	C_2	C_3
0.0060	1.12537	10,836.19437	43,206.60646

$$I = \frac{\alpha(T_t - T_b)A_e}{2\rho L_e} \quad (17)$$

where $T_t - T_b$ is the temperature differential across the thermoelectric plate, and ρ is the electrical resistivity of the thermoelectric element. Note that when HE2 is warmer than HE1, the current is positive, resulting in the Peltier effect adding heat to HE1 and removing heat from HE2; the reverse is also true. Joule heating within the module is assumed to distribute the heat equally into each heat exchanger. The rate of resistive heating in each heat exchanger is

$$\dot{Q}_{\text{resistive}} = \frac{1}{2}N\frac{I^2 L_e \rho}{A_e} \quad (18)$$

It is important to note that both the Peltier effect and Joule heating are far smaller in magnitude when compared with conduction, convection or radiative heat flow. Thus, these two modes of heat transfer could have been neglected with minimal effect on the power production. The Thomson effect can be neglected because the temperature fluctuations within the device are on the order of only a few degrees, resulting in a negligible change in the Seebeck coefficient [7,14,27].

Assuming that the thermoelectric plate does not store heat, is isolated from the environment, and that the energy removed from the system by electricity is negligible relative to the total energy flow [28], the change in temperature for HE1 is given by

$$\Delta T_b = \frac{\left(\dot{Q}_{fb} + \dot{Q}_{\text{cond}} + \dot{Q}_{\text{peltierHE1}} + \dot{Q}_{\text{resistive}}\right)}{\frac{M_b}{\text{MW}_b}C_{pb}}\Delta t \quad (19)$$

The change in temperature for HE2 during the day and the night, respectively, are

$$\Delta T_t = \frac{\left(\dot{Q}_{ft} + \dot{Q}_{st} - \dot{Q}_{\text{cond}} + \dot{Q}_{\text{peltierHE2}} + \dot{Q}_{\text{resistive}}\right)}{\frac{M_t}{\text{MW}_t}C_{pt}}\Delta t \quad (20)$$

$$\Delta T_t = \frac{\left(\dot{Q}_{ft} + \dot{Q}_{nt} - \dot{Q}_{\text{cond}} + \dot{Q}_{\text{peltierHE2}} + \dot{Q}_{\text{resistive}}\right)}{\frac{M_t}{\text{MW}_t}C_{pt}}\Delta t \quad (21)$$

where M_b and M_t are the masses of HE1 and HE2, respectively. The temperature differential across the thermoelectric plate is equal to $(T_t - T_b)$, assuming that the thermal resistance of the interface between the thermoelectric plate and the heat exchangers is insignificant [7]. Thus, the instantaneous electrical power output is given by

$$P = \frac{\alpha_e^2(T_t - T_b)^2 NA_e}{4\rho_e L_e} \quad (22)$$

The power density is obtained by dividing the instantaneous power output by the area of the thermoelectric plate.

3. Simulation results and discussion

In the lumped-parameter analysis, Bi $<<$ 1 corresponds to a body whose internal temperature is essentially uniform and therefore internal temperature gradients may be ignored. For a spherical body, Bi $\approx$ 0.1 corresponds to a surface temperature that is within 5% of the center temperature. At larger Biot numbers, the surface of the sphere equilibrates more quickly with the

surroundings than the center, resulting in a larger difference between the center and the surface temperatures and the lumped-parameter analysis is no longer valid. HE1 is designed to have a large thermal mass, which implies a large size, in order to suppress its rate of response to temporal variations in the temperature of the environment. Bi increases with length scale, hence it is not possible to simultaneously satisfy the requirements for both a large thermal mass and the lumped-parameter limit. In the current design, it is expected that the surface of HE1 equilibrates more rapidly with the surroundings than its center. However, the use of the lumped-parameter analysis in this work forces the center of the sphere to equilibrate with the surroundings as quickly as the surface.

The sizes of HE1, HE2 and the thermoelectric module were selected to obtain the smallest possible Biot number while maintaining a reasonable time step. HE1, the quartz sphere, has a diameter of 22 mm and is truncated at 17.6 mm from the bottom. Each of the four copper rods of HE2 has a diameter of 4.4 mm and a height of 88 mm. Each element of the thermoelectric has a cross-sectional area of 0.96 mm^2 resulting in a total module area of 245.2 mm^2. From their characteristic lengths, thermal conductivities, and heat transfer coefficients (Eqs. (3) and (4)), the Biot numbers for HE1 and HE2 are obtained as 0.29 and 0.00036, respectively. A Biot number of 0.29 results in a temperature difference between the center of a sphere and the surface of the sphere of about 15% [42].

Temperature and power output profiles for this geometry are shown in Fig. 2. It is seen in Fig. 2a that the air temperature experiences lower excursions than both HE1 and HE2 due to the radiative heat transfer HE2 experiences, and the consequent heat flow from HE2 to HE1 and vice versa. The temperature difference between HE1 and HE2 in Fig. 2b is just a few degrees. In Fig. 2b, the overshoot in the temperature differential when the temperature gradient is reversed arises from the radiation model used. When then sun sets below the horizon, HE2 instantaneously switches from receiving radiation from the sun to radiating to the night sky; similarly, when the sun rises above the horizon, HE2 instantaneously begins receiving solar radiation instead of emitting radiation. This temperature difference results in a fluctuating power density with a maximum of 1.16 W/m^2, an average of 0.164 W/m^2, and a minimum of 0 W/m^2. This corresponds to a maximum power output of 0.285 mW and an average power output of 0.04 mW, for the size of the thermoelectric selected (245.2 mm^2).

Because the hot and cold sides switch once during the diurnal cycle, the temperature differential $(T_t - T_b)$ where T_t and T_b are the temperatures of HE2 and HE1, respectively, experiences two zero-crossings during each 24-h period, and so the power production drops to zero at those two time instants. This diurnal cycle can be seen in Fig. 2b, where $(T_t - T_b)$ is positive for half of the day and negative for the other half of the day. During the daylight hours, HE2 receives heat from the sun via radiation, such that $(T_t - T_b) > 0$. During the night, HE2 emits heat to the night sky via radiation, such that $(T_t - T_b) < 0$. The temperature differential between the clear night sky in the desert and HE2 is greater than the temperature differential between the sun and HE2 during daylight hours. As a result, $(T_t - T_b)$ experiences a negative temperature excursion at night that is much larger in magnitude than its positive excursion during the day. The corresponding radiative heat flux scales as the fourth power of the temperature differential between the source and the sink. It is also seen in Fig. 2c that the frequency of the power curve is exactly equal to that of the diurnal temperature variation.

Fig. 3 shows the effect of scaling up the size of the device on the average power density, and the inset shows the effect of size scaling on the average and maximum power. Device size is changed by proportionately changing all length scales including the sphere radius, the size of the thermoelectric module, the radius of the rods,

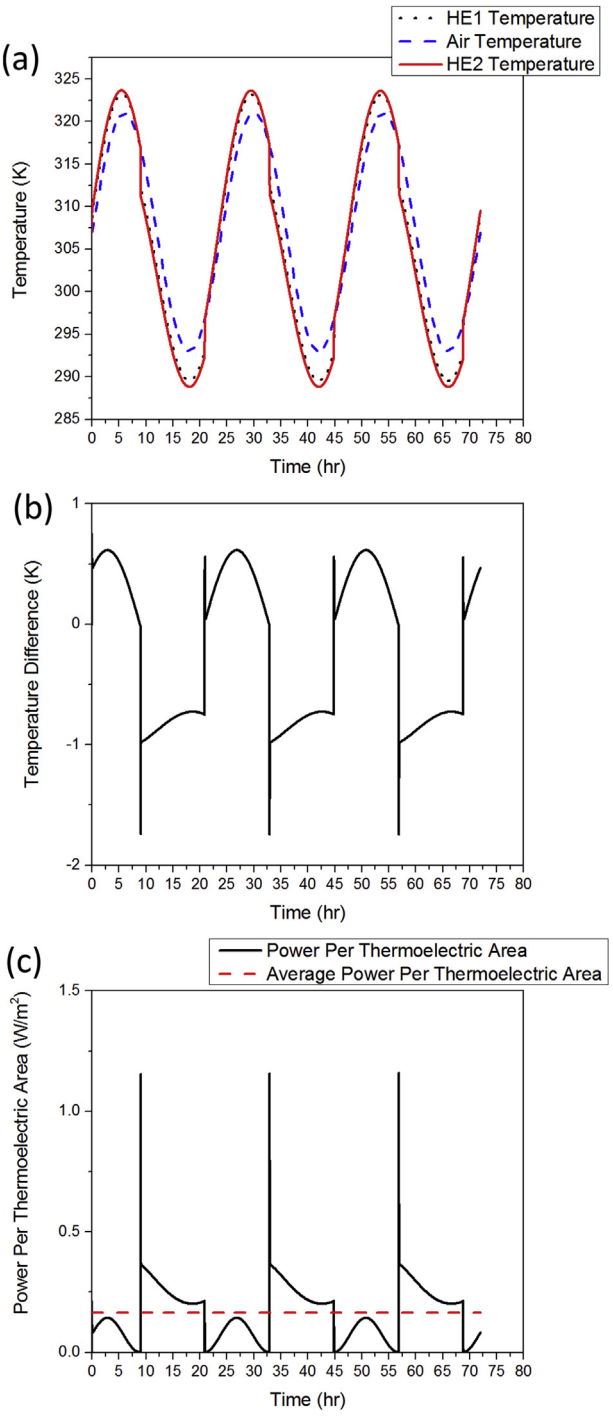

Fig. 2. (a) Temperature profiles for HE1, HE2, and the surrounding fluid; (b) resulting temperature difference $(T_t - T_b)$ across the thermoelectric; (c) instantaneous and time-averaged power density generated by the thermoelectric device.

and the lengths of the rods. The thermoelectric module's surface area is chosen as a representative dimension to indicate device size as this approximates the area the device would occupy on the ground. It is seen that the average power density increases rapidly with device size, reaches a maximum for a size of 2.03 m^2, and declines thereafter. The inset shows that an increase in size results in an increase in the temperature difference across the thermoelectric module and subsequently a larger power. As the device size increases further the thermal mass of HE2 also increases, reducing the temperature variation that the rods experience in response to

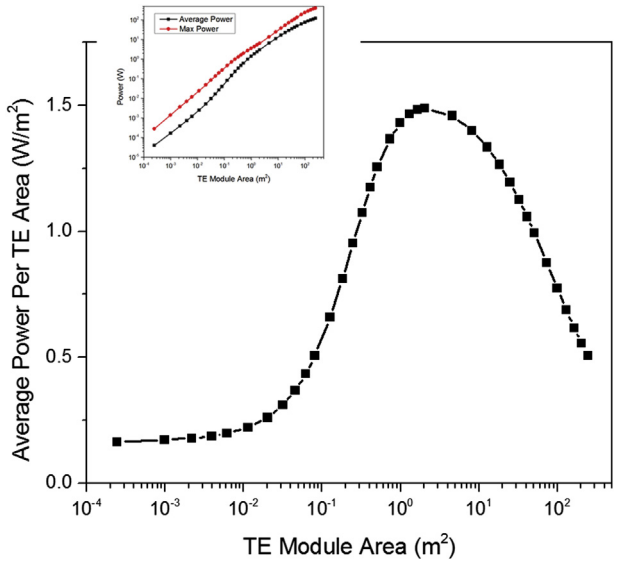

Fig. 3. Average power density produced by the thermoelectric module as a function of the thermoelectric module's surface area. Inset shows that power increases with size at small sizes.

the changing environment temperature. This effectively restricts the temperature difference across the thermoelectric module, and thus restricts the amount of power generated. As a result, the power out plateaus beyond 2 m^2, and the power density peaks at 2.03 m^2. It should be noted that although the lumped-parameter analysis may not be valid for larger device sizes, this only creates a temperature variation within HE1. This slightly affects the *magnitude* of the change in average power density with size, but the *trend* in the variation still holds. Additional optimization such as scaling the sizes of HE1 and HE2 independently, changing material type, and considering other thermoelectric module and heat exchanger geometries could result in a higher power density.

From these simulations, it is clear that using thermoelectrics in a thermally time-dependent environment produces relatively small amounts of power. Moreover, the power output is not steady. However, both shortcomings can be overcome by wiring several of these devices together and using recent advancements in power switching and electrical storage systems, leading to devices that could prove useful for remote power applications such as sensors and communication devices. Future experimental tests will be performed to validate these simulations, but this experimental work is beyond the scope of this paper.

Initial estimates suggest that the cost of materials to build these devices is less than $10. While other technologies certainly exist for larger-scale and less-expensive power generation for many applications, we believe that this approach is particularly useful when other power sources are not possible or reliable. In the proposed desert application, this approach offers the advantage over solar photovoltaics of greater mechanical robustness, immunity to coverage by dust storms, and night-time generation. Miniaturized, portable versions of these devices could be designed to power sensors on passive robots probing remote environments and tracking beacons for shore birds, fish, and other wildlife whose movements cause temporal temperature changes. While Fig. 3 shows that smaller sizes produce less power, we can optimize other design features to generate more power for small devices. For example, increasing either the surface area-to-volume ratio of HE2 via surface roughening, or adding thermal insulation to HE1 would increase the amount of power generated for a fixed device size. In addition to optimizing for the geometry and materials for a given size, one must also consider the rate at which the fluid changes temperature. A device operating on the concepts presented here could be designed to exploit the temperature fluctuations in the human bloodstream to power sensors for health monitoring or mechanisms for targeted drug delivery by considering exotic materials and suitable geometries that generate an adequate temperature gradient from thermal variations occurring on a faster time scale.

4. Conclusions

A model for a thermoelectric power generator in a temporally-varying temperature environment was developed. A heat transfer model was constructed that considers the time-dependent convective and radiative heat exchange between the environment and the device. The device employs two heat exchangers, each made of different materials and having a different geometry, such that a temporal temperature gradient in the environment can be converted into a spatial temperature gradient within the device. It was shown that the generated spatial temperature gradient is suitable for power generation. The power generation is proportional to the spatial temperature gradient, which is dependent on heat exchanger geometry, material, and the environment's time-varying temperature profile. The power output of the device undergoes significant temporal fluctuations as dictated by the corresponding temperature fluctuations in the environment. We demonstrated that for the diurnal temperature variation in Death Valley, CA during the summer, an average power density of approximately 0.46 W/m^2 is possible for a thermoelectric device with a size of 2.45 cm^2. A scaling study on the device size indicates that there exists an optimal size for which the power density is maximized. The results presented here confirm that thermoelectric power generation in a temporally-varying temperature environment is a reliable power source for remote power applications.

Acknowledgements

This authors wish to acknowledge funding from the University of Delaware Research Foundation through its Strategic Initiatives Program. Additionally, financial support for P. A. through the NSF-NUE Program (0939283) is acknowledged.

References

[1] S.W. Angrist, Direct Energy Conversion, fourth ed., Allyn and Bacon, Inc., Boston, 1982.
[2] S. Riffat, Applied Thermal Engineering 23 (2003) 913–935.
[3] J. Chen, Journal of Applied Physics 79 (1996) 2717.
[4] G. Chen, Journal of Applied Physics 109 (2011) 104908.
[5] D. Kraemer, B. Poudel, H.-P. Feng, J.C. Caylor, B. Yu, X. Yan, Y. Ma, X. Wang, D. Wang, A. Muto, K. McEnaney, M. Chiesa, Z. Ren, G. Chen, Nature Materials 10 (2011) 532–538.
[6] M. Telkes, Journal of Applied Physics 25 (1954) 765.
[7] J. Henderson, in: Intersociety Energy Conversion Engineering Conference, vol. 2, American Chemical Society, Boston, 1979, pp. 1835–1840.
[8] D.M. Rowe, G. Min, Journal of Power Sources 73 (1998) 193–198.
[9] C. Wu, Applied Thermal Engineering 16 (1996) 63–69.
[10] T. Kyono, R.O. Suzuki, K. Ono, IEEE Transactions on Energy Conversion 18 (2003) 330–334.
[11] J. Yang, F.R. Stabler, Journal of Electronic Materials 38 (2009) 1245–1251.
[12] J. Yu, H. Zhao, Journal of Power Sources 172 (2007) 428–434.
[13] J. Esarte, G. Min, D.M. Rowe, Journal of Power Sources 93 (2001) 72–76.
[14] F. Meng, L. Chen, F. Sun, Energy 36 (2011) 3513–3522.
[15] H. Glosch, M. Ashauer, U. Pfeiffer, W. Lang, Sensors and Actuators A Physical 74 (1999) 246–250.
[16] A.I. Hochbaum, R. Chen, R.D. Delgado, W. Liang, E.C. Garnett, M. Najarian, A. Majumdar, P. Yang, Nature 451 (2008) 163–167.
[17] J.M. Zide, D.O. Klenov, S. Stemmer, A.C. Gossard, G. Zeng, J.E. Bowers, D. Vashaee, A. Shakouri, Applied Physics Letters 87 (2005) 112102.
[18] R.O. Suzuki, D. Tanaka, Journal of Power Sources 124 (2003) 293–298.

[19] L. Chen, J. Gong, F. Sun, C. Wu, International Journal of Thermal Sciences 41 (2002) 95–99.
[20] D.K. Benson, C.E. Tracy, in: Proceedings of the Fourth International Conference on Thermoelectric Energy Conversion, Arlington, TX, 10–12 March 1982, IEEE, New York, 1982, pp. 11–14.
[21] P.M. Mayer, R.J. Ram, Nanoscale and Microscale Thermophysical Engineering 10 (2006) 143–155.
[22] L. Chen, J. Li, F. Sun, C. Wu, Applied Energy 82 (2005) 300–312.
[23] A. Şişman, H. Yavuz, Energy 20 (1995) 573–576.
[24] J. Chen, Z. Yan, L. Wu, Journal of Applied Physics 79 (1996) 8823.
[25] J. Chen, C. Wu, Journal of Energy Resources Technology 122 (2000) 61.
[26] K. Yazawa, A. Shakouri, Journal of Applied Physics 111 (2012) 024509.
[27] Y. Meydbray, R. Singh, A. Shakouri, in: ICT 2005. 24th International Conference on Thermoelectrics, 2005, IEEE, 2005, pp. 348–351.
[28] J.W. Stevens, Energy Conversion and Management 42 (2001) 709–720.
[29] D.T. Crane, G.S. Jackson, Energy Conversion and Management 45 (2004) 1565–1582.
[30] G. Min, D.M. Rowe, Journal of Power Sources 38 (1992) 253–259.
[31] K. Yazawa, A. Shakouri, Environmental Science & Technology 45 (2011) 7548–7553.
[32] D.R. Gaskell, Introduction to the Thermodynamics of Materials, fifth ed., Taylor & Francis Group, LLC, New York, 2008.
[33] Momentive Performance Materials Quartz Inc.. http://www.quartz.com/gedata.html, 2007.
[34] J.R. Howel, R. Siegel, M.P. Menguc, Thermal Radiation Heat Transfer, fifth ed., Taylor and Francis Group, LLC, Boca Raton, FL, 2011.
[35] The Engineering ToolBox, http://www.engineeringtoolbox.com/thermal-conductivity-d_429.html (n.d.).
[36] S. Scherrerand, H. Scherrer, in: D.M. Rowe (Ed.), CRC Handbook of Thermoelectrics, first ed., CRC Press, Inc., New York, 1995, pp. 211–239.
[37] The Engineering ToolBox, http://www.engineeringtoolbox.com/dry-air-properties-d_973.html (n.d.).
[38] R.B. Bird, W.E. Stewart, E.N. Lightfoot, Transport Phenomena, second ed., John Wile & Sons, Inc., New York, 1924.
[39] D.R. Poirier, G.H. Geiger, Transport Phenomena in Materials Processing, The Minerals, Metals & Materials Society, Warrendale, 1994.
[40] W.A. Gray, R. Muller, Engineering Calculations in Radiative Heat Transfer, first ed., Pergamon Press, New York, 1974.
[41] Omar Reis. http://www.tecepe.com.br/scripts/AlmanacPagesISAPI.dll, 2004.
[42] M.N. Oziski, Basic Heat Transfer, McGraw-Hill, 1977.